RSC Advances

PAPER

View Article Online
View Journal | View Issue

Cite this: *RSC Adv.*, 2026, **16**, 21765

Solvation of copper(II), zinc(II) and lead(II) in monoethanolamine solutions attained *via* leaching of microwave-assisted-roasted sulfidic tailings

Nor Kamariah, [ab] Sai Manoj Gali, [a] Koen Binnemans [b] and Jeroen Spooren *[a]

Solvometallurgical leaching using lixiviants based on monoethanolamine (MEA) was investigated for extracting copper, zinc, and lead from sulfidic tailings that underwent an optimized short microwave-assisted roasting pre-treatment. The addition of 0.5 M ammonium sulfate to the MEA solvent increased the extraction efficiencies for all targeted metals, as it provided charge balancing for the cationic metal–MEA complexes. Similar extraction efficiencies were found for copper (~67%), zinc (70%), and lead (~66%), highlighting the capability of the MEA-based lixiviant to dissolve the anglesite phase ($PbSO_4$) present in the roasted tailings, which is poorly soluble in pure water (~1.5%). Additionally, microwave-assisted leaching at a high temperature (of 150 °C) increased the degree of dissolution of the remaining unroasted sphalerite phases (ZnS), but decreased the leaching yield for copper. Furthermore, addition of water to the MEA solvent did not affect the copper and zinc leachability at 60 °C but lowered the dissolution of lead and iron. The dissolution behavior of metals salts in MEA–water mixtures was fostered by experimentally determining the Gibbs free energy of transfer values, which in turn were compared with theoretical binding energies obtained *via* Density Functional Theory (DFT) calculations. DFT calculated binding energies compared well with the experimental Gibbs free energy of transfer for the dissolution of metal salts in MEA–water mixtures, entailing that the complex binding energy has a strong contribution to the overall dissolution of Gibbs free energy of the metal cations in the studied solvents.

Received 27th January 2026
Accepted 15th April 2026

DOI: 10.1039/d6ra00733c

rsc.li/rsc-advances

1. Introduction

Sulfidic tailings are leftover materials generated during the production of copper, zinc, lead, and other sulfide-bearing minerals from their ores. In Europe alone, the annual production of these tailings is estimated at about 500 million metric tonnes, with historical accumulations totaling approximately 28 000 million metric tonnes, making them the largest volume of tailings in Europe.[1] Inadequate management of sulfidic tailings can lead to serious environmental issues. These tailings are rich in residual sulfide minerals, such as pyrite, which can generate acid mine drainage (AMD) when oxidized by air or bacteria. This generation of AMD produces highly acidic solutions with dissolved metals and the accumulation of heavy metals, posing a potential risk of soil and groundwater contamination.[2,3]

Despite the environmental risks associated with them, these tailings can be utilized as a secondary resource because they may still contain substantial amounts of valuable metals that were not recovered during the beneficiation process, such as copper, zinc, cobalt, and lead. In some cases, the metal contents in the tailings may even be as high as those found in primary ore deposits, which are experiencing grade depletion in recent decades.[4,5] Therefore, reprocessing sulfidic tailings can benefit to minimize environmental problems and to serve as an alternative source of metals.

Currently, valuable metals are generally extracted from ores by pyrometallurgical and/or hydrometallurgical processes. Pyrometallurgy involves high temperatures (300–1600 °C) to treat high-grade ores, thereby taking advantage of the maximum thermal efficiency during the heat-exchange operations. Meanwhile, hydrometallurgy employs lower temperatures (<200 °C) and is usually applied to extract metals from low-grade ores or secondary sources. Metal leaching, as a primary process in hydrometallurgy, commonly uses acids (*e.g.* sulfuric acid) as leaching agents. However, hydrometallurgical leaching with acids usually suffers from poor selectivity, as metal impurities are often co-dissolved together with the targeted metals.

Solvometallurgy, on the other hand, applies non-aqueous solutions with little or no water present to extract and recover metals. Solvometallurgy is a relatively new approach in extractive metallurgy and offers several advantages over conventional hydrometallurgy, such as minimal water consumption leading to reduced wastewater generation, and higher leaching selectivity.[6] This increased selectivity is particularly beneficial for

[a]*Materials and Chemistry, Flemish Institute for Technological Research (VITO N.V.), Boeretang 200, 2400 Mol, Belgium. E-mail: jeroen.spooren@vito.be*
[b]*KU Leuven, Department of Chemistry, Celestijnenlaan 200F, Box 2404, 3001 Leuven, Belgium*

treating low-grade ores, mine tailings, or industrial process residues.[6] Some solvometallurgical processes have been suggested for the recovery of metals from sulfidic tailings. These include leaching in alcoholic ammoniacal systems to selectively extract copper, zinc, and lead,[7] as well as the application of ion flotation to recover copper from dilute ammoniacal leachates.[8]

Monoethanolamine (MEA; $HOC_2H_4NH_2$), also known as 2-aminoethanol or ethanolamine, is classified as an organic solvent belonging to the group of the amino alcohols (or alkanolamines), and thus possesses a molecular structure characterized by the presence of both an amine and a hydroxyl functional group. This bifunctionality contributes to its versatility, enabling applications in various industries. MEA is widely applied in gas treatment processes, specifically as a solvent for CO_2 capture, and finds applications in the production of wood preservatives and surfactants.[9–11] Despite its widespread use in various industries, and its amino alcohol characteristics in facilitating the formation of complexes with metal ions,[12–14] documented applications of MEA in extractive metallurgy remain scarce, with the available instances primarily focusing on applications in aqueous systems. For instance, the addition of aqueous MEA as a stabilizing agent for copper(II) ions in thiosulfate leaching solutions, aimed to prevent thiosulfate oxidative degradation caused by copper(II) ions through the formation of several copper–MEA complexes (*i.e.* $[Cu(MEA)_2]^{2+}$, $[Cu(MEA)_3]^{2+}$, $[Cu(MEA)_4]^{2+}$), has enabled the optimal extraction of silver from silver sulfide up to 80%.[15] A similar investigation also reported the role of MEA as the leaching agent in dissolving silver by forming silver–MEA complexes.[16] In another study, aqueous solutions of mono-, di-, and triethanolamine were employed to extract and recover lead from lead sulfate present in waste batteries.[17] MEA, as a bidentate ligand, allows for a variety of binding modes with metal cations, which will eventually determine the solubility and stability of the resulting complexes. In a study involving copper(II) ions and an ethanolammonium perchlorate solution, mono- and diethanolamine molecules were observed to coordinate with the metal ion through their nitrogen atoms.[18] The study proposed that the weak coordination of the hydroxyl groups of ethanolamines was influenced by steric effects, creating competition with solvated water molecules. Additionally, the study noted that the Cu–MEA complex exhibited higher acidity compared to the complex of copper–ammonia, attributing this difference to the strong steric influence of the hydroxyl groups of ethanolamines on the coordinated water molecules. In another study, ethanolamines were reported to act as multidentate ligands *via* their amine, hydroxyl, and deprotonated hydroxyl groups when forming complexes with copper(II) in a solution containing ethanolammonium nitrate.[19] Stable complexes were obtained at basic pH, even with a low ratio of ligand to metal ion. However, precipitation of copper(II) hydroxide did occur when the solution reached a neutral pH with a low ratio of ligand to metal ion. The bidentate ligand characteristic of MEA toward copper(II) ions was reported in a study by Caumul *et al.*, wherein they predicted the possible complex structure to adopt a square planar form.[20] This configuration resembled the type of complex formed between copper(II) ions and ethylenediamine, where the Jahn–Teller distortion hindered copper(II) ions from forming six-coordinated complexes. Other studies also proposed that bidentate coordination occurs in the complexation of MEA with zinc(II) and lead(II) ions, resulting in the formation of $[Zn(MEA)_3]^{2+}$ and $[Pb(MEA)_2]^{2+}$ or $[Pb(MEA)_3]^{2+}$, respectively.[21,22] Whereas, the stability of complexes of MEA with copper(II), cobalt(II), and nickel(II) in a mixed aqueous system exhibited increased stability constants, particularly with the addition of cosolvent methanol, acetonitrile, dimethylformamide (DMF), and dioxane.[23] This enhanced stability was attributed to the improved control over the solvation of reacting species through a combination of water and cosolvent molecules, as opposed to relying solely on water.

In recent studies, we have demonstrated the selective extraction of copper from chrysocolla and lead from zinc calcine by means of (non-aqueous) MEA–ammonium salt solutions.[24,25] It was demonstrated that the dissolution of copper(II) ions from chrysocolla is facilitated through the complexation with the nitrogen from MEA and causes a reduced solubility of silica-containing matrix material.[24] Furthermore, lead, existing in the form of anglesite ($PbSO_4$), could be selectively extracted from zinc calcine material through complexation of the bivalent lead cation with MEA molecules, presenting an alternative method for addressing the challenging dissolution of anglesite in hydrometallurgical leaching processes.[25]

Sulfide minerals typically serve as the primary hosts for valuable metals within tailings. Pyrite (FeS_2), pyrrhotite ($Fe_{(1-x)}S$), sphalerite (ZnS), chalcopyrite ($CuFeS_2$), galena (PbS), covellite (CuS), and arsenopyrite (FeAsS) are among the main sulfide minerals commonly found in tailings.[26] Roasting is often employed as a pre-treatment to oxidize stable sulfide minerals into their respective oxide and/or sulfate minerals, to enhance their extraction efficiency.[27,28] In a prior study, we found that roasting of sulfidic tailings at temperatures ranging from 500 °C to 550 °C for 1 hour by means of microwave (MW) heating successfully converted most of chalcopyrite and sphalerite, *i.e.* the main copper- and zinc-bearing minerals in the tailings, into their respective sulfate and/or oxide mineral phases.[27] Simultaneously, the conversion of pyrite, the main iron-bearing minerals in the tailings, into sulfate minerals at the same temperature range was comparatively lower, which was intended to minimize the dissolution of iron impurities during leaching. The simultaneous hydrometallurgical extraction of copper, zinc and lead from roasted sulfidic tailings is hindered by the scarce solubility of $PbSO_4$ in water.[29] Thus, MEA is an ideal candidate solvent to achieve such simultaneous extraction, and has not been investigated previously.

In this work, we have utilized a combination of microwave heating treatments and a solvometallurgical leaching system to achieve high extraction efficiency, selectivity, and kinetics for copper, zinc, and lead from sulfidic tailings. The optimization of MW-assisted roasting of sulfidic tailings involved varying roasting temperatures and times. Simultaneously, the leaching of the roasted tailings in MEA was to our knowledge investigated for the first time and optimized by introducing ammonium salts and employing different leaching techniques, temperatures, and reaction times. Finally, Density Functional

Theory (DFT) calculations investigated the metal–MEA complex coordination in the absence and presence of water to support experimental observations with theoretical modelling.

2. Materials and methods

2.1 Chemicals and materials

Sulfidic tailings samples were provided by SOMINCOR Lundin Mining from the tailings storage facility of the Neves Corvo mine (Portugal). Monoethanolamine (MEA, 99%) was purchased from Fisher Scientific. Ammonium sulfate ($(NH_4)_2SO_4$, ≥99.0%) and ammonium chloride (NH_4Cl, ≥99.5%) were purchased from Sigma-Aldrich and used as received. In solubility tests the following metal sulfates were used: $CuSO_4$ (anhydrous, 98%, Thermo Scientific), $PbSO_4$ (≥98.0%, Aldrich), $Fe_2(SO_4)_3$ (NORMAPUR, VWR), $ZnSO_4 \cdot 7H_2O$ (≥99.5%, Merck), $FeSO_4 \cdot 7H_2O$ (≥99.0%, VWR), whereby the former two were used as received and the latter three were dehydrated in an oven at 105 °C until constant mass. The metal oxides used were CuO (98%, Sigma-Aldrich), ZnO (99.9%, Sigma-Aldrich), PbO (99.9%, Alfa Aesar) and Fe_2O_3 (anhydrous, VWR). The other tested solvents were methanol (water content < 0.1%, VWR), ethanol (water content < 0.1%, VWR), and *n*-butanol (water content < 0.1%, VWR). Hydrochloric acid (HCl) 37% (VWR), nitric acid (HNO_3) 65% (Chem-Lab NV), tetrafluoroboric acid (HBF_4) 50% (Fisher Scientific), multi-element standards (LabKings) and Milli-Q® water (18.2 MΩ cm at 25 °C, TOC < 5 ppb) were used during solid sample digestion and preparation of leachate solutions for inductively coupled plasma-optical emission spectroscopy (ICP-OES) analyses.

2.2 Analyses

To determine the mineralogical composition of the initial and roasted tailings samples, as well as the leaching residues, X-ray powder diffraction (XRD) analysis was conducted using a PANalytical Empyrean diffractometer equipped with a cobalt anode operating at 40 kV and 45 mA. Continuous mode scans, with a scanning speed of 0.010° s^{-1} and a step size of 0.04° in the 2θ range of 5–120°, were applied. Qualitative and quantitative analyses of the diffractograms were conducted using HighScore Plus software with TiO_2 (Kronos International) serving as an external standard for calibration.

For the determination of the chemical compositions of the tailings and the metal concentrations in pregnant leach solutions (PLS), ICP-OES was performed on a PerkinElmer® Avio 500 spectrometer. The ICP-OES spectrometer featured axial (AX)/radial (RAD) dual plasma view options, a GemTip Cross-Flow II nebulizer, and an Elemental Scientific prepFAST autosampler. For solid samples, digestion in HCl, HBF_4 and HNO_3 at 105 °C for 2 hours using a Digiprep Block Digestion System (SCP Science) preceded ICP-OES analysis. Liquid samples obtained from leaching underwent centrifugation and syringe-filtration before being pipetted into a DigiTUBE vessel for subsequent MEA evaporation and acid digestion. The final solutions (obtained from both solid and liquid samples) were diluted with Milli-Q® water, acidified with a 5% HNO_3 solution, and then measured in triplicate by ICP-OES. Fourier transform infrared spectroscopy (FT-IR) analyses were performed on a Nicolet 10 (Thermo Scientific) equipped with a diamond crystal. The measurements were performed in attenuated reflectance (ATR) mode. The spectrum is recorded in 32 scans for the range 4000 cm^{-1} to 400 cm^{-1} with a resolution of 4 cm^{-1}. The sample preparation consisted of mixing 0.2 g of an anhydrous metal sulphate salt with 150 μL of pure MEA, which was left to stand for 1 h before FT-IR measurement of the wetted powder.

2.3 Experimental procedures

To enhance the extractability of the targeted metals (copper, zinc, lead) for leaching, roasting treatments were performed to convert sulfide bearing-minerals in the tailings into their sulfates and/or oxides. Prior to roasting, the initial tailings underwent drying at 40 °C until a constant mass was achieved under a nitrogen flow to prevent oxidation of the samples. Subsequently, the dried tailings samples were finely crushed into powders (with a mean particle size of 19 μm ± 1 μm, a d_{50} = 7.7 μm ± 0.3 μm and d_{90} = 57 μm ± 6 μm, as determined by Microtrac S3500) using a mortar and pestle. Following this, the powdered samples were put in alumina crucibles and roasted in air in duplicate in a microwave furnace operating in multimode (Milestone PYRO advance; magnetron frequency of 2450 MHz; magnetron output of 2 × 950 W; cavity dimension of 43 cm (width) × 40 cm (depth) × 41 cm (height)). The roasting was conducted at 550 °C, with a ramp time of 30 min and dwell times of 15 min and 30 min at each temperature. The maximum MW power was set at 1800 W, and the furnace was equipped with a silicon carbide (SiC) plate at the top of the heating chamber to ensure that the temperature inside the chamber reached the set temperature.

In order to predict the dissolution behavior of the targeted metals present in the roasted tailings, preliminary solubility tests were conducted using synthetic systems. These tests involved anhydrous metal sulfates ($CuSO_4$, $ZnSO_4$, $PbSO_4$, $Fe_2(SO_4)_3$) and metal oxides (CuO, ZnO, PbO, Fe_2O_3) in a series of selected alcohols (methanol, ethanol, *n*-butanol) and MEA. The amount of salt added was adjusted to reach the maximum solubility of each salt in the respective solvent (reaching saturation point). The procedure involved pipetting the solvents into tubes, followed by the addition of salt. The mixtures were then shaken in an overhead shaker at ambient temperature (20–25 °C, 1 atm) overnight. Subsequently, the mixtures were filtered using syringe filters (0.45 μm) and were prepared for ICP-OES analysis. All solubility tests were executed in duplicate, and the presented error bars indicate the standard deviations of the means derived from the duplicate experiments. Similarly, the solubility of anhydrous $PbSO_4$, $ZnSO_4$, $CuSO_4$ and $FeSO_4$ were tested in different MEA–water mixtures with a known volume to volume ratio.

Leaching of the roasted tailings was conducted using pure MEA and combinations of MEA with different ammonium salts (*i.e.*, sulfate and chloride salts) at different concentrations, as well as water addition at different ratios. Leaching was performed at both room temperature and elevated temperature.

Room temperature leaching was conducted in a sealed glass vial with a magnetic stirrer placed on a multi-position magnetic stir plate at a liquid-to-solid (L/S) ratio of 10 mL g^{-1} and a constant stirring speed of 500 rpm. Whereas, leaching at elevated temperature was carried out using either a conventional water bath system or a microwave system (Flexiwave Milestone®). The leaching parameters of temperature and time were optimized while keeping the L/S ratio and stirring speed constant. Each leaching test was carried out in duplicate, and the presented error bars indicate the standard deviations of the means derived from the duplicate experiments. Finally, the roasted tailings were also leached at 60 °C for 1 hour by heating of the reaction vials in a water bath in MEA–water mixtures with and without the addition of ammonium salts (*i.e.*, 3 M NH_4Cl or 0.5 M $(NH_4)_2SO_4$). Following leaching, the solid residues were separated from the PLS by syringe-filtration. The PLS was then prepared for ICP-OES analysis. Leaching efficiency (LE (%)) was calculated according to eqn (1):

$$\text{LE } (\%) = \frac{C_M \times V_l}{C_i \times m_i} \times 100 \quad (1)$$

where C_M is the metal concentration in the PLS (mg L^{-1}); V_l is the volume of lixiviant used for leaching (L); C_i is the initial metal concentration in the roasted tailings sample (mg kg^{-1}); m_i is the roasted tailings mass used for leaching (kg).

Density functional theory (DFT) calculations were performed using the Gaussian 16 program[30] at the B3LYP/LANL2DZ level of theory for all molecular optimizations, employing the CPCM implicit solvation model. Binding energies were calculated using eqn (2);

$$E_{BB} = E_{Com} - (E_M + E_F) \quad (2)$$

where E_{Com}, E_M and E_F correspond to the total energies of the metal-fragment coordination complex, isolated metal atom and isolated molecular fragments (MEA or water), respectively, including the zero-point energy corrections. Calculations on metal-fragment coordination complexes and isolated metal atoms were performed by considering a net charge of +2, with multiplicity of zero (singlet) using Grimme's empirical dispersion (GD2) correction.[31] Bond order analysis was performed on optimized metal-coordination complexes, employing the NBO/Wiberg methodology,[32] as implemented in the Gaussian 16 program.

3. Results and discussion

3.1 Characterization of sulfidic tailing materials

Pyrite constituted the predominant mineral phase identified by XRD present in the tailings, accounting for 43.7 wt% (Fig. 1). It was followed by quartz (28.9 wt%) and chamosite (21.3 wt%). Siderite (2.7 wt%), muscovite (2.6 wt%), and tetrahedrite (0.8 wt%) were present in smaller quantities. Notably, sphalerite (ZnS) was the only detectable zinc-containing mineral phase. Due to their low concentrations, minerals containing copper and lead could not be detected by XRD. Consistent with the mineralogical characterization, chemical analysis by ICP-OES showed iron (Fe) (26.4 wt%) and sulfur (S) (24.5 wt%) as the predominant elements in the tailings (Table 1). Copper accounted for 0.4 wt%, zinc for 1.0 wt%, and lead for 0.4 wt%.

In our previous study, Mineral Liberation Analysis (MLA) findings indicated that sulfide minerals predominantly host copper, zinc, and lead in the tailings.[27] Specifically, chalcopyrite emerged as the primary copper-bearing mineral, and sphalerite and galena as the main zinc and lead-bearing mineral phases,

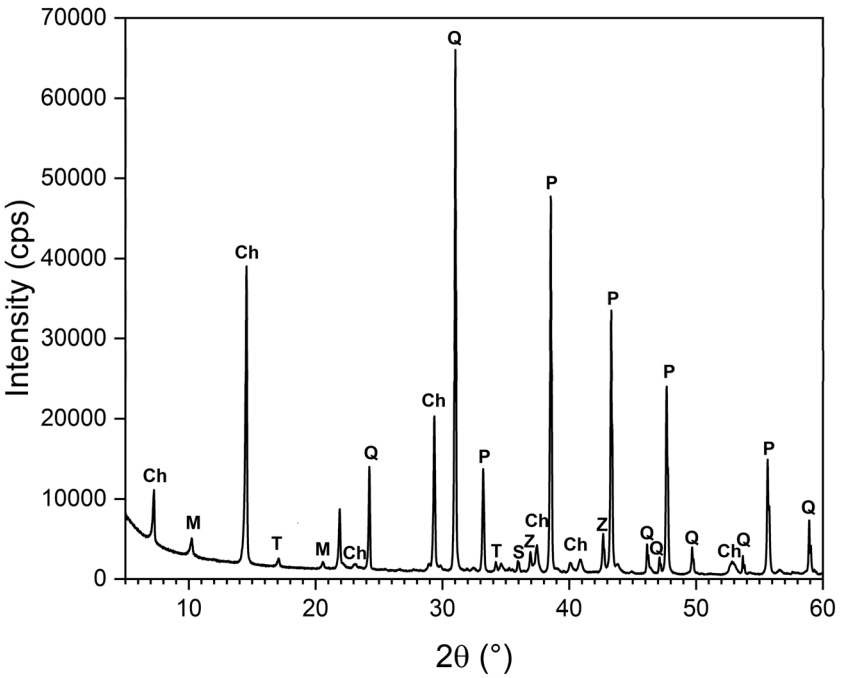

Fig. 1 XRD diffractogram of the Neves Corvo sulfidic tailings (Ch = chamosite; M = muscovite; P = pyrite; Q = quartz; S = siderite; T = tetrahedrite; Z = zinc-bearing mineral (sphalerite)).

Table 1 Elemental composition of the Neves Corvo sulfidic tailings as measured by ICP-OES[a]

Element	Concentration (ppm)
Fe	264 000
S	244 500
Zn	10 360
Cu	3515
Pb	3970
Mg	9520

[a] Tested in duplicate and reported data are mean values.

respectively. Given that the metals of interest were present as sulfide minerals, it is anticipated that roasting, as a pretreatment, will be necessary to enhance the extractability of these metals during leaching by converting the sulfide phases into their sulfate and/or oxide mineral counterparts.

3.2 Solubility tests of metal and ammonium salts in MEA

An initial screening test explored the use of molecular organic solvents from the alcohol group and MEA as potential leaching agents for extracting copper, zinc and lead from oxidative roasted sulfidic tailings, which contain these metals, along with iron, in their sulfate and oxidic forms. To predict the dissolution behavior of such metal sulfates and oxides, solubility tests were conducted on anhydrous metal sulfates and metal oxides in the alcohols methanol (MeOH), ethanol (EtOH) and *n*-butanol (*n*-BuOH), as well as monoethanolamine (MEA). For comparison with aqueous leaching systems, the solubility of these salts in pure water was also examined. The results of the solubility tests are presented in Table 2.

As summarized in Table 2, only water and MEA demonstrated the ability to dissolve all four anhydrous metal sulfates. $CuSO_4$ exhibited the highest solubility in water (8.7×10^{-2} M), surpassing its solubility in MeOH (2.7×10^{-2} M) and MEA (1.3×10^{-2} M) by more than 3 and 6 times, respectively. Similarly, $ZnSO_4$ displayed solubilities in water more than 11 and 17 times higher than in MEA and MeOH, respectively. $PbSO_4$ was found to be insoluble in monofunctional alcohols (MeOH, EtOH and *n*-BuOH), while its solubility in bifunctional MEA (1.1×10^{-2} M) was approximately 70 times higher than in water. $Fe_2(SO_4)_3$ exhibited partial solubility in all solvents, with its concentration in MEA being 23 times lower than in water.

In comparison, metal oxides showed low solubility. The solubilities of ZnO and PbO in MEA were 9 and 69 times higher, respectively, than in water. This low-to-no solubility towards iron species, combined with its relatively high solubility for copper(II), zinc(II), and especially lead(II) sulfates and oxides, positions MEA as the most promising candidate tested in this study for developing an efficient and selective solvometallurgical system for leaching copper, zinc, and lead with minimal liberation of iron impurities. Based on these results, MEA was selected as the solvent for further investigation in a leaching process using actual tailing materials from Neves Corvo, aiming to achieve high leaching efficiency and selectivity.

Furthermore, as demonstrated in our previous study, incorporating certain ammonium salts can be beneficial in improving the extraction efficiency and selectivity for certain metals.[24] It was shown that ammonium chloride could be dissolved in higher concentrations (≤4 M) in MEA compared to ammonium carbonate (≤2 M) and ammonium sulfate (≤1 M) at room temperature.[24] The higher solubility of ammonium chloride could be due to its lower lattice enthalpy (708 kJ mol^{-1})[33] in contrast to the lattice enthalpies of ammonium carbonate (2153 kJ mol^{-1})[34] and ammonium sulfate (1766 kJ mol^{-1}),[35] resulting in higher dissolution of chloride salt caused by stronger anion–dipole interaction with MEA. Expanding on these findings, the current study involves leaching optimizations of roasted tailings, not only in pure MEA, but also in MEA–ammonium salts as leaching agents.

3.3 MEA leaching of roasted tailings

Based on our earlier microwave-assisted roasting optimization studies,[27] the effect of roasting time of 15 min and 30 min at 550 °C on MEA-leaching was investigated. In the initial optimization step, the leaching efficiencies in pure MEA at room temperature were examined for varying MW-assisted roasting times of sulfidic tailings (Fig. 2). Extending roasting times from 15 min to 30 min did not significantly impact copper extraction but slightly increased zinc extraction. Sphalerite, the main zinc mineral, transforms into sulfate minerals at higher temperatures than chalcopyrite, the main copper mineral.[27] Chalcopyrite begins converting to soluble copper(II) sulfate at 320 °C and decomposes to stable copper(II) oxide at 500–550 °C.[36] Thus, longer roasting times favour zinc extraction and decrease copper leaching due to increased production of soluble zinc(II) sulfate and stable copper(II) oxide, respectively. Also, iron co-

Table 2 Solubility of metal sulfate anhydrates salts and metal oxides

Salt	$CuSO_4$	$ZnSO_4$	$PbSO_4$	$Fe_2(SO_4)_3$	CuO	ZnO	PbO	Fe_2O_3
Solvent	Cu (M)	Zn (M)	Pb (M)	Fe (M)	Cu (M)	Zn (M)	Pb (M)	Fe (M)
H_2O	8.7×10^{-2}	1.5×10^{-1}	1.6×10^{-4}	1.7×10^{-1}	—	6.6×10^{-5}	6.5×10^{-5}	—
MeOH	2.7×10^{-2}	8.7×10^{-3}	—	5.9×10^{-3}	—	—	1.3×10^{-3}	—
EtOH	2.0×10^{-4}	1.1×10^{-5}	—	2.8×10^{-2}	—	—	—	—
BuOH	—	—	—	6.2×10^{-4}	—	—	—	—
MEA	1.3×10^{-2}	1.3×10^{-2}	1.1×10^{-2}	7.3×10^{-3}	7.9×10^{-5}	6.1×10^{-4}	4.5×10^{-3}	—

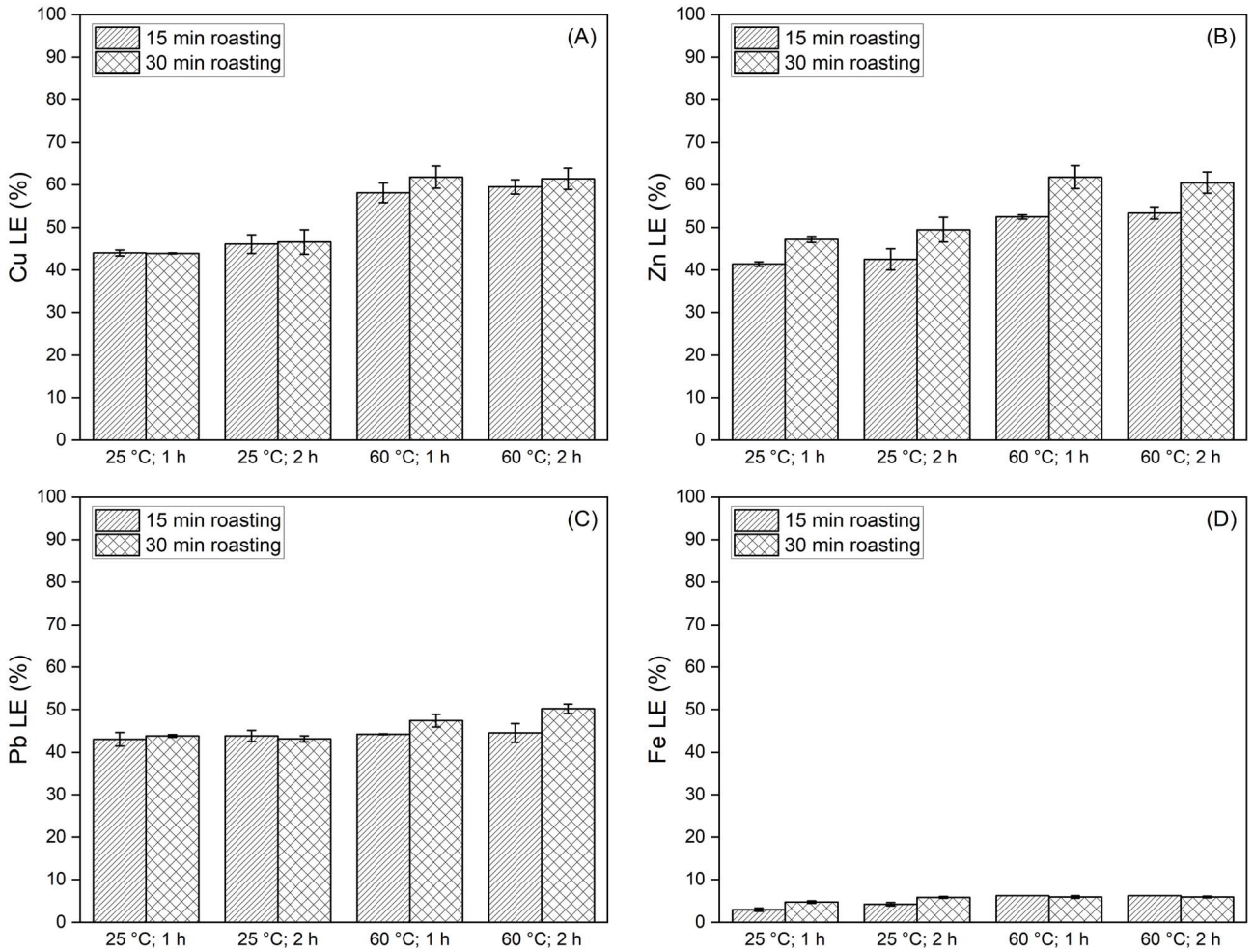

Fig. 2 Effect of leaching time temperature on the extraction efficiencies of targeted metals (A) copper, (B) zinc, (C) lead and (D) iron in pure MEA (L/S = 10 mL g^{-1}; stirring speed = 500 rpm) from a sulfidic tailings sample MW-assisted roasted at 550 °C at two different dwell times.

dissolution slightly increased upon longer roasting time, indicating a higher presence of iron sulfate phases and hence rendered leaching less selective. Moreover, extending the leaching time from 1 to 2 hours did not yield significant increases in the extraction efficiencies of the metals of interest.

The effect of temperature on metal leaching from roasted tailings in pure MEA was investigated next. In general, leaching at 60 °C yielded higher extraction efficiencies for the targeted metals compared to room temperature leaching, as depicted in Fig. 2. The enhanced leachability is ascribed to the positive effect on the reaction rate, stemming from the exponential dependence between the rate constant and temperature according to the Arrhenius equation.[37] Also at 60 °C, extending the leaching time from 1 to 2 h did not significantly increase the extraction efficiencies (Fig. 2). Meanwhile, the leaching of iron at 60 °C and 2 hours demonstrated a more notable increase as it nearly doubled with respect to leaching at room temperature, indicating reduced selectivity for copper, zinc and lead leaching. In the overall observation for leaching in pure MEA, the most optimal extraction efficiencies were achieved for tailings roasted at 550 °C for 30 min and leached at 60 °C for 1 hour. This condition resulted in the highest extractions of 62% for copper, 62% for zinc, and 47% for lead, with a co-dissolution of 6.0% iron.

In previous studies we also showed that addition of ammonium chloride or ammonium sulfate to a MEA lixiviant could enhance the extraction efficiency of copper, as well as that of zinc and lead, respectively.[24,25] The anions from these salts have the varying ability in serving as charge balancers to stabilize the positively charged metal–MEA complexes. Therefore, the addition of either ammonium chloride (NH_4Cl 3 M) or ammonium sulfate ($(NH_4)_2SO_4$ 0.5 M) to the MEA lixiviant for leaching at 60 °C for 1 hour was tested. The chosen salt concentrations were derived from the same previous studies. Additionally, to take advantage of MEA's high boiling point (170 °C), leaching was also conducted at an elevated temperature of 150 °C using MW heating, enabling a shortened leaching time of 15 min.

As shown in Fig. 3(A), the addition of 0.5 M $(NH_4)_2SO_4$ at 60 °C leaching for 1 hour increased the extraction of copper, zinc and lead to 67%, 70% and 66%, respectively, while reducing the co-dissolution of iron to 4.7%. Leaching with the same salt addition under microwave heating at 150 °C for 15 min

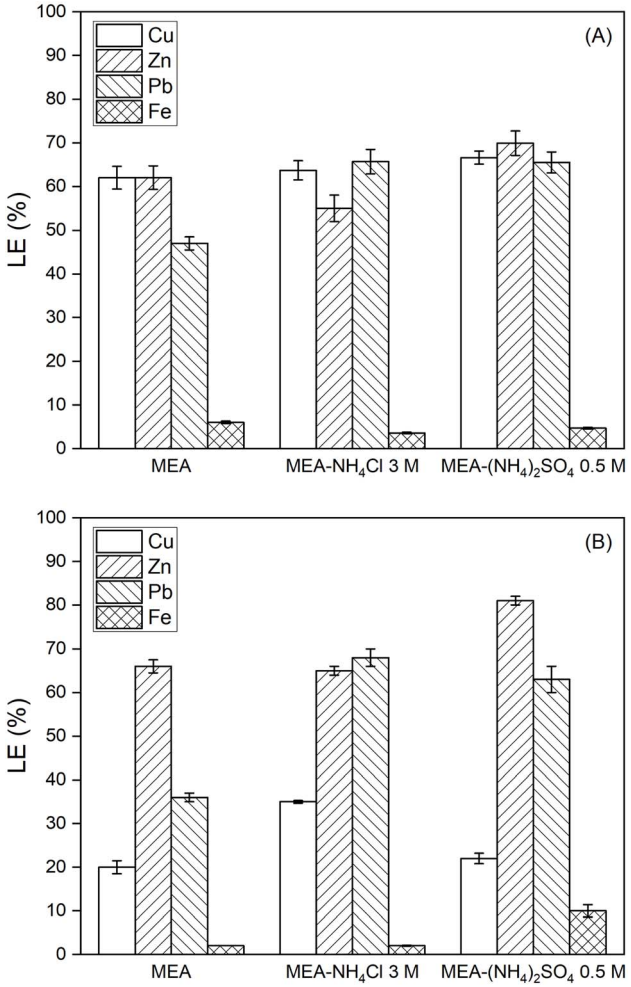

Fig. 3 Effect of ammonium salt additions on the extraction efficiencies of Cu, Zn, Pb and impurities Fe: (A) a mild leaching temperature (conventional leaching; $T = 60$ °C; $t = 1$ h; L/S = 10 mL g^{-1}; stirring speed = 500 rpm), (B) a high leaching temperature (MW-assisted leaching; $T = 150$ °C; $t = 15$ min; L/S = 10 mL g^{-1}; stirring speed = 500 rpm).

achieved the highest zinc extraction of 81% (Fig. 3(B)), whereas the extraction of lead almost doubled compared to its extraction in pure MEA. Furthermore, the addition of 3 M NH_4Cl to MEA led to enhanced extraction of copper and lead, but not zinc, at both investigated leaching temperatures of 60 °C and 150 °C. Further research is needed to investigate the factors influencing the varying ability of these salts to stabilize the formed metal–MEA complexes.

Fig. 4 shows a detail of the XRD diffractograms of the leaching residues after MEA–$(NH_4)_2SO_4$ 0.5 M leaching at 60 °C in a water bath and at 150 °C in a MW system. The main difference between both leaching residues lies in the disappearance, after leaching at 150 °C, of magnetite (Fe_3O_4) phases, which were replaced by the appearance of magnesium ferrite ($MgFe_2O_4$) phases. Magnetite, formed as an intermediate during the oxidation of pyrite according to eqn (2) and (3), is typically unstable and tends to undergo further oxidation into more stable iron-bearing phases under stronger oxidizing condition. Both magnetite and hematite were present in the roasted tailings (Fig. 4) and leaching at a mild temperature (60 °C) did not alter the presence of these phases. However, during MW-assisted leaching at 150 °C, it is hypothesized that the oxidation and substitution of an iron(II) cation in the magnetite phases with a magnesium(II) cation occurs, resulting in the formation of a spinel magnesium ferrite structure. Furthermore, similar substitutions of the iron(II) cation in magnetite with other metal ions such as zinc, manganese, cobalt, and nickel have been reported in other studies.[38–40]

Additionally, magnesium ferrite has been reported in various studies to have the capability to adsorb copper(II) ions, which could cause the lower copper leaching in MW-leaching at 150 °C.[41–43] Alternatively, it could also be hypothesized that copper anions reduced to metallic copper at 150 °C with MEA acting as a reducing agent. Feng *et al.* tested the reduction of $CuCl_2$, CuCl, CuO and Cu_2O in MEA at 120–150 °C to metallic copper.[44] Although the copper chloride salts did indeed form metallic copper at increasing temperature, the copper redissolved upon cooling to room temperature, whereas copper oxides fully converted to stable metallic copper nanoparticles at 120 °C. Nevertheless, both hypotheses could not be verified by XRD characterization due to the low copper concentrations in the solid residue. Furthermore, the XRD diffractogram also revealed a lower intensity of the sphalerite phase in the MW leaching residue compared to the intensity in the conventional leaching residue, indicating that higher temperature leaching could dissolve remaining unroasted sphalerite, resulting in higher zinc extraction efficiency upon MW-assisted leaching (81%) compared to conventional leaching (70%).

Based on the results, the optimal extraction efficiencies for all targeted metals are achieved by leaching at a mild temperature of 60 °C for 1 hour using MEA–$(NH_4)_2SO_4$ 0.5 M, yielding 67% for Cu, 70% for Zn, and 66% for Pb. It resulted in the co-dissolution of iron at 4.7%, slightly higher than that produced with MEA–NH_4Cl 3 M, but lower (indicating higher selectivity) than leaching in pure MEA. However, MW-assisted leaching has the advantage of dissolving a larger portion of remaining sphalerite phases, resulting in an increased zinc extraction efficiency. Nonetheless, the transformation of magnetite phases into magnesium ferrite phases during MW-leaching might adsorb the dissolved copper(II) ions. This advantage, therefore, comes at the expense of lower copper efficiency during the MW-assisted leaching. An alternative approach to overcome this is by employing a two-step leaching process. Initially, leaching at 60 °C is conducted to maximize copper extraction, and subsequently, the residue from the first leaching step is subjected to a second leaching using fresh lixiviant in the MW at 150 °C to dissolve the remaining sphalerite phases and extract more zinc. Insights from previous Fourier transform infrared spectroscopy (FTIR) studies on MEA–metal complexes could serve as an indicator of the occurring leaching mechanisms for the roasted tailings material.[24,25] Herein, copper leaching involved the interaction of copper ions with amine ligands of MEA to form the positively charged copper–amine complex,[24] while zinc and lead leaching occurred through the coordination of zinc and lead ions with MEA molecules through both amine and

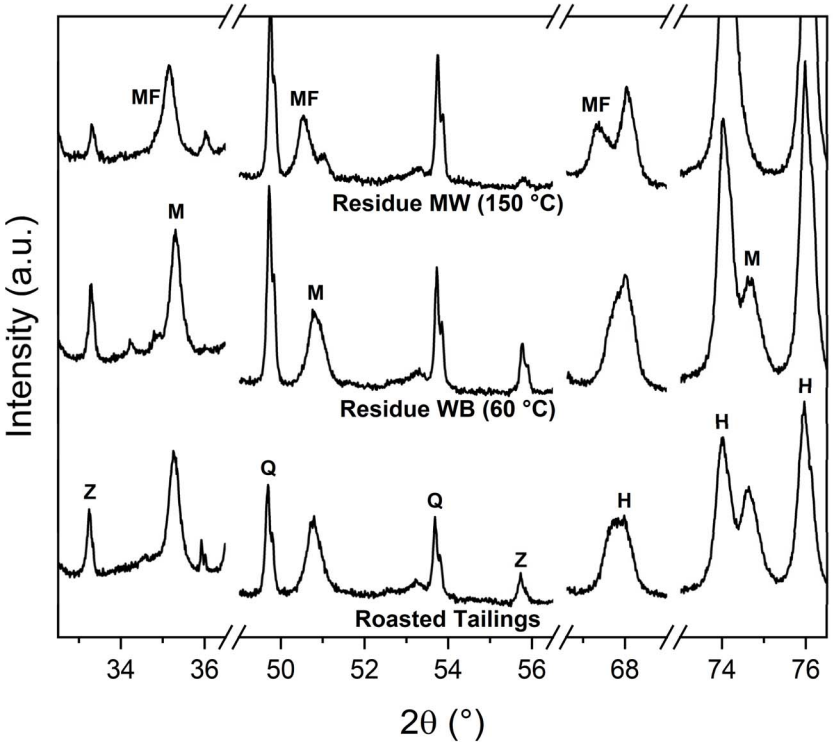

Fig. 4 XRD diffractograms of: roasted tailings, residue of conventional leaching in MEA–$(NH_4)_2SO_4$ 0.5 M ($T = 60$ °C; $t = 1$ h; L/S = 10 mL g^{-1}; stirring speed = 500 rpm), and residue of MW-assisted leaching in MEA–$(NH_4)_2SO_4$ 0.5 M ($T = 150$ °C; $t = 15$ min; L/S = 10 mL g^{-1}; stirring speed ≈ 500 rpm) (H = hematite; M = magnetite; MF = magnesium ferrite, Q = quartz; Z = zinc-bearing mineral (sphalerite)).

hydroxyl ligands.[25] The additions of ammonium chloride and ammonium sulfate provided counter anions to stabilize the complex formed in solution. The observed differences in leachability resulting from the addition of different ammonium salts in this study are generally attributed to the varying ability of salt-forming anions to balance the formed cationic metal–MEA complexes. However, the exact roles of the anion species (*i.e.*, SO_4^{2-} and Cl^-), and ammonium ions (NH_4^+) in the dissolved metal ion complex formation still require further investigation.

3.4 Effect of water addition to MEA on metal ion solubility

Variations in solvent compositions can result in differences in solvation properties, leading to distinct distribution properties of metal ions in solutions. The addition of water to a non-aqueous system, given that water is a better electron donor compared to the majority of non-aqueous solvents, has the potential to preferentially coordinate metal ions and alter the dissolution behavior of metal ions in the mixed system.[45] Conversely, adding a non-aqueous solvent to an aqueous system can also modify the extraction behavior of metal ions. This addition can change the dielectric constant, affecting the stability of the formed complexes, change the mutual solubility in the two phases, or influence the interfacial tensions.[45] Therefore, the effect of water–MEA mixtures at different ratios on the dissolution behavior of copper, zinc, lead and iron were investigated to further tailor their eventual extraction from roasted tailings.

To achieve the aforementioned purpose, the dissolution behavior of synthetic metal salts ($CuSO_4$, $ZnSO_4$, $PbSO_4$, $FeSO_4$) in different MEA–water mixtures was first determined. As illustrated in Fig. 5(A), the addition of water to MEA led to a decrease in solution pH and an enhancement in the dissolution of copper. A similar pattern was also evident in Fig. 5(B), where the use of the mixed system resulted in higher zinc dissolution compared to pure MEA. Meanwhile, the presence of MEA in the mixed system enhanced lead dissolution compared to that in pure water, with the highest lead dissolution achieved by the combination of 50% (v/v) from both solvents (Fig. 5(C)). As for iron, its dissolution was reduced with the presence of MEA in the mixed system, lower than that in pure water, except in the case of about 65% (v/v) of MEA in water, where it exhibited iron dissolution comparable to that in pure water (Fig. 5(D)).

While it is challenging to establish a direct correlation between solvent compositions and their solvation behavior using a single factor, a study conducted by Kalidas *et al.* proposed the concept of solvent medium effect to understand solute behavior in both pure and mixed solvents.[46] The medium effect measures the change in the total solvation energy when a solute is transferred from one solvent to another, thereby influencing the stability and complexation characteristics of the solute in the two solvents. This effect is directly related to the standard molar Gibbs free energy (ΔG°) for transferring the

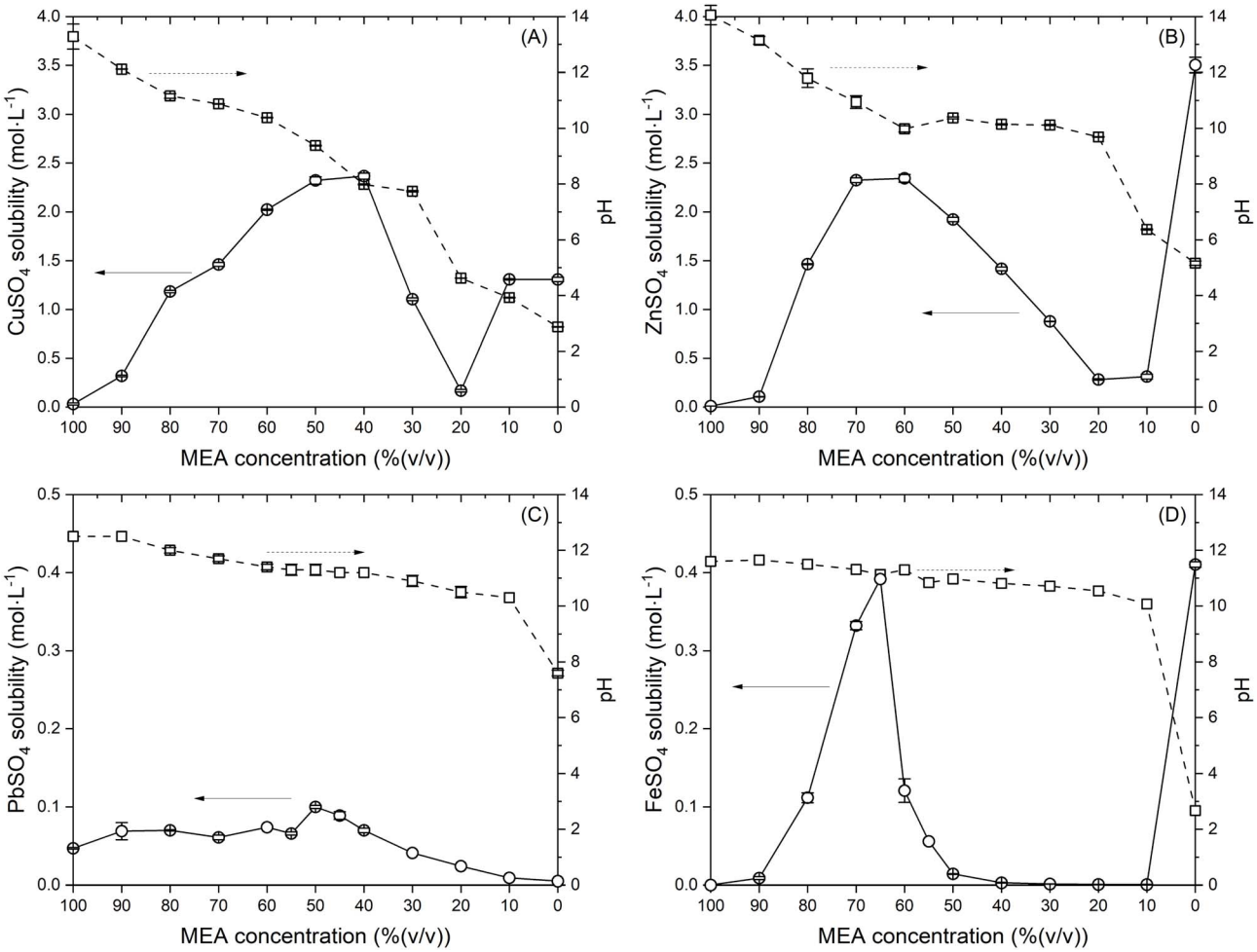

Fig. 5 Effect of different compositions of MEA and water (% v/v) mixed system on the dissolution of: (A) $CuSO_4$, (B) $ZnSO_4$, (C) $PbSO_4$, (D) $FeSO_4$ (T = room temperature).

solute from one to another solvent. As an illustration, the medium effect of transfers from water to water + methanol, as well as from water to water + ethanol, was reported for alcohol groups. For both alcohols, it was reported that the values of ΔG° for copper(II), zinc(II), and lead(II) became increasingly positive as the alcohol concentrations in the mixed system rose, corresponding to a less favorable solvation of these ions by the mixed system compared to that in pure water.[46]

Using the average solubility data of the metal salts in MEA–water mixtures from Fig. 5, the medium effect or Gibbs free energy of transfer ($\Delta_t G^{\circ}$) of electroneutral salts is calculated according to eqn (3):

$$\Delta_t G^{\circ} = 2.303 \times R \times T \times \left[pK_{sp}^{\circ}(\text{MEA} + \text{water}) - pK_{sp}^{\circ}(\text{water}) \right] \quad (3)$$

whereby R is the ideal gas constant, T temperature, $K_{sp}^{\circ}(\text{MEA} + \text{water})$ and $K_{sp}^{\circ}(\text{water})$ the solubility products of the salt in MEA + water and water, respectively, and $pK_{sp}^{\circ} = -\log K_{sp}^{\circ}$. The results are presented in Fig. 6. From this figure, it is observed that, generally, the Gibbs free energy of transfer of lead sulfate dissolution yields lower values than the

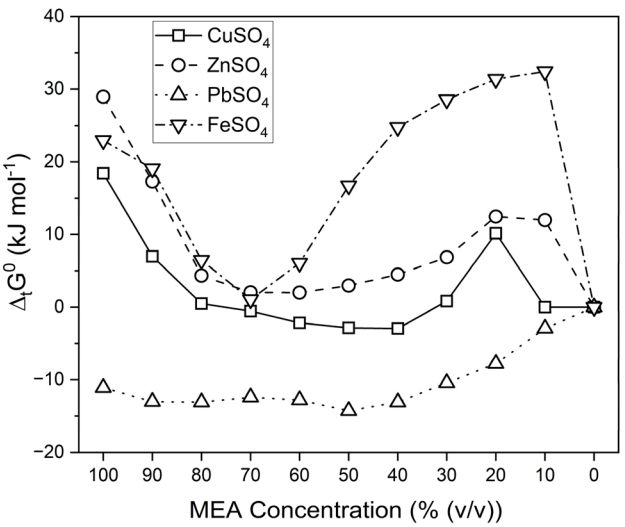

Fig. 6 Gibbs free energy of transfer for salt dissolution in different compositions of MEA and water (% v/v).

dissolution of other salts across all solvent compositions. The figure highlights that the dissolution of lead sulfate in pure MEA and a combination of MEA + water exhibits lower Gibbs free energies compared to lead dissolution in only water, signifying favorable dissolution in pure MEA, or MEA + water. In contrast, when compared to the dissolution of iron sulfate, that exhibits the larger Gibbs free energies of transfer, it indicates less favorable dissolution, offering possibilities for achieving selective leaching.

To better understand the observed dissolution behavior of the studied metal salts in MEA and MEA + water mixtures, DFT calculations were performed to evaluate the binding energies, of dissolved metal cation complexes in the studied solvents, together with an analysis on their bond orders, to extract structure-free energy relationships and to understand the role of ligands and their coordination to metal cations in modulating the Gibbs free energies of metal MEA and water (% v/v) complexes as reported in Fig. 7. Firstly, DFT calculations were performed to determine the most stable coordination of MEA molecules with the studied metal cations in a pure MEA solvent. To this end, Cu–MEA, Zn–MEA, Fe–MEA and Pb–MEA metal-fragment coordination complexes, consisting of 3, 4 and 6 MEA fragments, were simulated to replicate either a tetrahedral or an octahedral coordination environment.

Calculations for $[M(MEA)_y]^{2+}$ complexes, whereby M represents the metal cation (Cu/Zn/Fe/Pb) and $y = 4$ or 6, were performed on structures consisting of both metal–N (–NH_2 unit of MEA fragment) and metal–O (–OH unit of MEA fragment) coordination. For $[M(MEA)_y]^{2+}$ with $y = 2$ or 3, structures were also generated such that the MEA molecule acts as a bidentate ligand with both –NH_2 and –OH units of the MEA fragment coordinating with the metal atom. See SI Fig. SI-1–SI-3 for details. MEA coordinates similarly with Cu^{2+}, Fe^{2+} and Zn^{2+} cations, preferring an octahedral coordination compared to tetrahedral counterparts, as they generated comparatively lower binding energies. More specifically, the octahedral $[Zn(MEA)_6]^{2+}$ complex is stable by ~22 kcal mol^{-1} when compared to tetrahedral $[Zn(MEA)_4]^{2+}$ complex and the octahedral $[Fe(MEA)_6]^{2+}$ complex is stable by ~60 kcal mol^{-1} when compared to tetrahedral $[Fe(MEA)_4]^{2+}$ complex; see Fig. SI-1 and SI-2 for details. In comparison, the octahedral $[Cu(MEA)_6]^{2+}$ complex is stable by ~24 kcal mol^{-1} when compared to tetrahedral $[Cu(MEA)_4]^{2+}$ complex. Also, for the monodentate coordination with 6/4 MEA molecules a considerably lower binding energy was obtained for

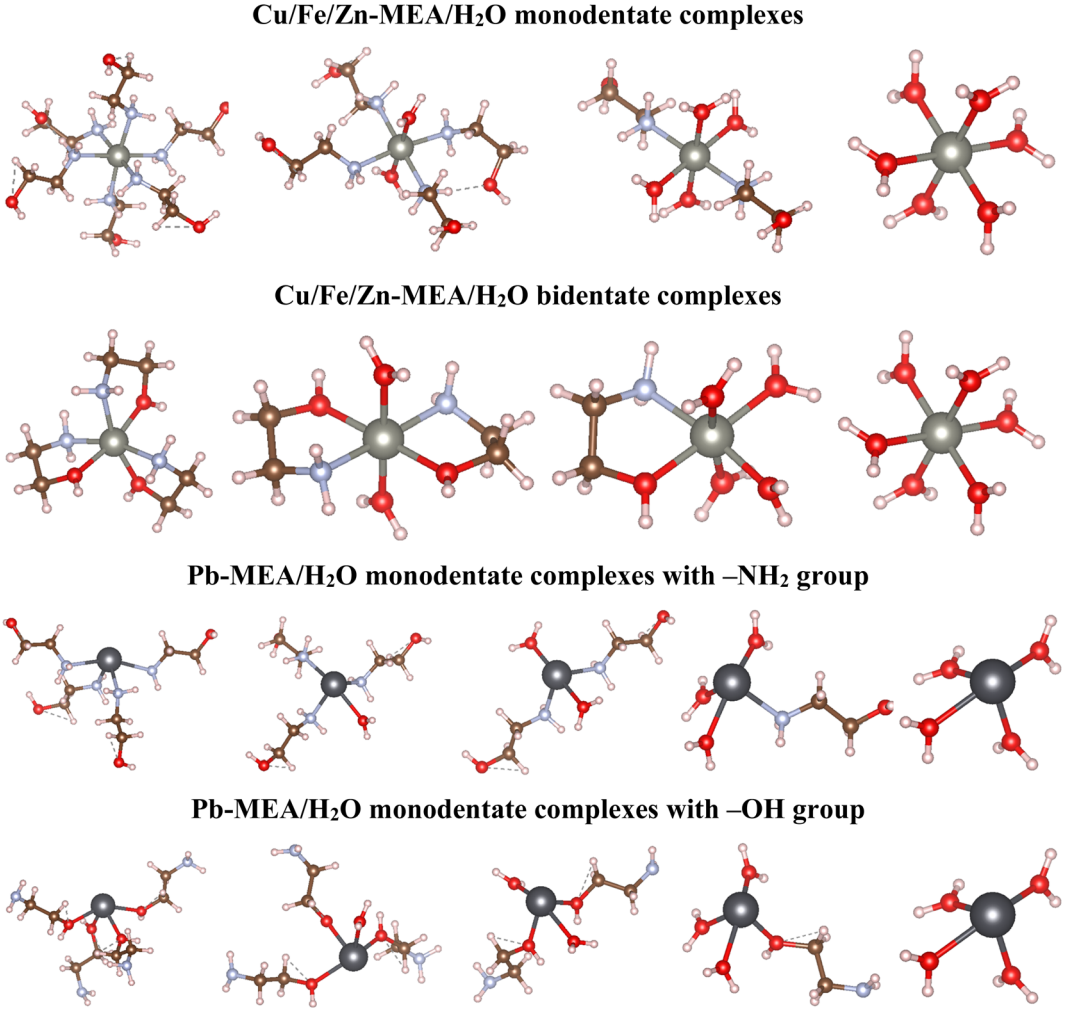

Fig. 7 Complex coordination modes modelled by DFT for metal–MEA/H_2O complexes of zinc(II), iron(II) and lead(II).

$[M(MEA)_{6/4}]^{2+}$ complexes, of the order of ~15 kcal mol^{-1} for $[Zn(MEA)_{6/4}]^{2+}$ complexes, ~30 kcal mol^{-1} for $[Fe(MEA)_{6/4}]^{2+}$ complexes and ~18 kcal mol^{-1} for $[Cu(MEA)_{6/4}]^{2+}$ complexes, when coordination took place *via* the electron donating nitrogen atoms of the amine groups when compared to the complexes where coordination took place *via* the electron withdrawing oxygen atoms of the hydroxyl groups. Furthermore, for both copper(II), iron(II) and zinc(II) cations, $[M(MEA)_3]^{2+}$ complexes wherein 3 MEA molecules formed a bidentate octahedral coordination with metal cations and $[M(MEA)_6]^{2+}$ complexes wherein 6 MEA molecules formed a monodentate octahedral coordination with metal cations generated similar DFT binding energies, as reported in the SI (Fig. SI-1 and SI-2), implying that the coordination environment together with steric effects contribute to the overall stability of the mono- and bidentate metal–MEA complexes.

In the case of Pb–MEA complexes, however, asymmetric tetrahedral complexes were found to be more stable. Pb coordination with 6 MEA molecules showed high structural distortions and cleavages of metal–ligand coordination bonds upon DFT structural optimizations; see Fig. SI-3 for details. The tetrahedral monodentate Pb–MEA complexes were also more stable when coordination took place *via* the nitrogen atom of the $-NH_2$ group, similar to those found for Zn/Fe–MEA complexes. Stabilization of asymmetric tetrahedral complexes could be attributed to the easy accommodation of stereochemically active $6s^2$ lone pair, reducing electron repulsion and stabilizing the structure,[47] and possibly also due to better orbital overlap.[48]

Taking the most stable DFT optimized geometries, as reported above, mono- and bidentate octahedral coordination complexes for copper(II), zinc(II) and iron(II) and the tetrahedral monodentate coordination for lead(II) complexes, wherein coordination occurred *via* the electron donating nitrogen atoms of the amine groups, were selected to calculate the binding affinities for different MEA–water ratios as represented in Fig. 7. These binding energies were obtained from DFT calculations involving full geometry optimization followed by a frequency analysis, wherein the frequency calculations were also used to verify that each optimized structure corresponds to a true local minimum on the potential energy surface, as evidenced by the absence of imaginary vibrational frequencies. Although the frequency calculations provide complete thermochemical information, including zero-point energy (ZPE), vibrational/rotational/translational entropy, and the thermal Gibbs free energy, only the ZPE-corrected electronic energies were employed in the present work. Entropy contributions ($-T\Delta S$) were therefore not included. This choice is consistent with common practice in comparative binding-energy studies of strongly bound coordination complexes,[49,50] where entropic terms are typically small relative to the enthalpic component and tend to cancel when comparing structurally similar species.

In analogy to the Gibbs free energy of transfer (eqn (3)), the difference in binding energy with respect to a fully hydrated metal cation was calculated according to eqn (4).

$$\Delta E_{BB} = [E_{BB}(\text{MEA/MEA + water}) - E_{BB}(\text{water})] \quad (4)$$

where, E_{BB}(MEA) is the binding energy of monodentate $[M(MEA)_{6/4}]^{2+}$ complex for M = Cu/Zn/Fe/Pb or bidentate $[M(MEA)_3]^{2+}$ complex for M = Cu/Zn/Fe, E_{BB}(MEA + water) is the binding energy of partially hydrated metal–MEA–water complex and E_{BB}(water) is the binding energy of fully hydrated $[M(H_2O)_{6/4}]^{2+}$ complex for M = Cu/Zn/Fe/Pb. The difference in binding energies, hitherto referred to as relative binding energies with respect to fully hydrated metal–water complex (ΔE_{BB}), as reported in Fig. 8, were calculated by gradually replacing the MEA molecules from metal–MEA complexes with water molecules, as schematically represented from left to right in Fig. 7.

More specifically, the DFT binding energies for monodentate Cu/Zn/Fe–MEA + water complexes were reported for $[M(MEA)_6]^{2+}$, $[M(MEA)_4(H_2O)_2]^{2+}$, $[M(MEA)_2(H_2O)_4]^{2+}$ complexes relative to $[M(H_2O)_6]^{2+}$ complex and for bidentate Cu/Zn/Fe–MEA + water complexes were reported for $[M(MEA)_3]^{2+}$, $[M(MEA)_2(H_2O)_2]^{2+}$, $[M(MEA)_1(H_2O)_4]^{2+}$ complexes relative to $[M(H_2O)_6]^{2+}$ complex. Furthermore, the Fig. 8 also shows the $[Pb(MEA)_{4-y}(H_2O)_y]^{2+}$ complexes which were evaluated and whereby the coordination with the –OH and $-NH_2$ groups were also investigated.

The binding energies in $[Pb(MEA)_{4-y}(H_2O)_y]^{2+}$ complexes are significantly lower when MEA binds to the lead cation *via* its amine group rather than with its hydroxyl group, entailing that the amine bound complexes are relatively stable. As a result, the ΔE_{BB} values of the $-NH_2$ bounded $[Pb(MEA)_{4-y}(H_2O)_y]^{2+}$ complexes are negative and their evolution with respect to the MEA concentration in water (Fig. 8(C)) evolves similar to the experimentally determined ΔG_t (Fig. 6). For zinc and iron cation complexes with MEA + water, the bidentate bounded MEA complexes show generally a slightly lower overall binding energy than the monodentate bound MEA complexes, in line with the slightly higher Wiberg bond orders observed in bidentate complexes, as reported in SI: Tables SI-1 and SI-2. More specifically, the relative binding energies of bidentate $[Zn(MEA)_3]^{2+}$ and monodentate $[Zn(MEA)_6]^{2+}$ complexes were higher than the $[Zn(H_2O)_6]^{2+}$ complexes (Fig. 8(B)). When the MEA molecules in Zn–MEA complexes were partially substituted by water molecules, their relative binding energies were comparatively lower. For Fe–MEA complexes, on the other hand, the relative binding energies of both $[Fe(MEA)_3]^{2+}$ and $[Fe(MEA)_6]^{2+}$ complexes were lower than for the $[Fe(H_2O)_6]^{2+}$ complex. When the MEA molecules in Fe–MEA complexes were partially substituted by water molecules, their relative binding energies are further lowered when compared to the parent $[Fe(MEA)_3]^{2+}$ and $[Fe(MEA)_6]^{2+}$ complexes. Furthermore, the $[Fe(MEA)_4(H_2O)_2]^{2+}$ complex, whereby MEA bounding *via* only the $-NH_2$ groups takes place, has a minimal binding energy with respect to otherwise coordinated complexes (Fig. 8(D)). Interestingly, these variations in relative binding energies of zinc and iron cation complexes with MEA + water closely follow the variations in net Wiberg bond orders (see SI for details), with the partially hydrated complexes showing the highest bond orders entailing that the bonding strength and ligand field effects are higher for partially hydrated complexes. In conjunction with the variations observed in net Wiberg bond orders, the drop in binding energies observed in partially

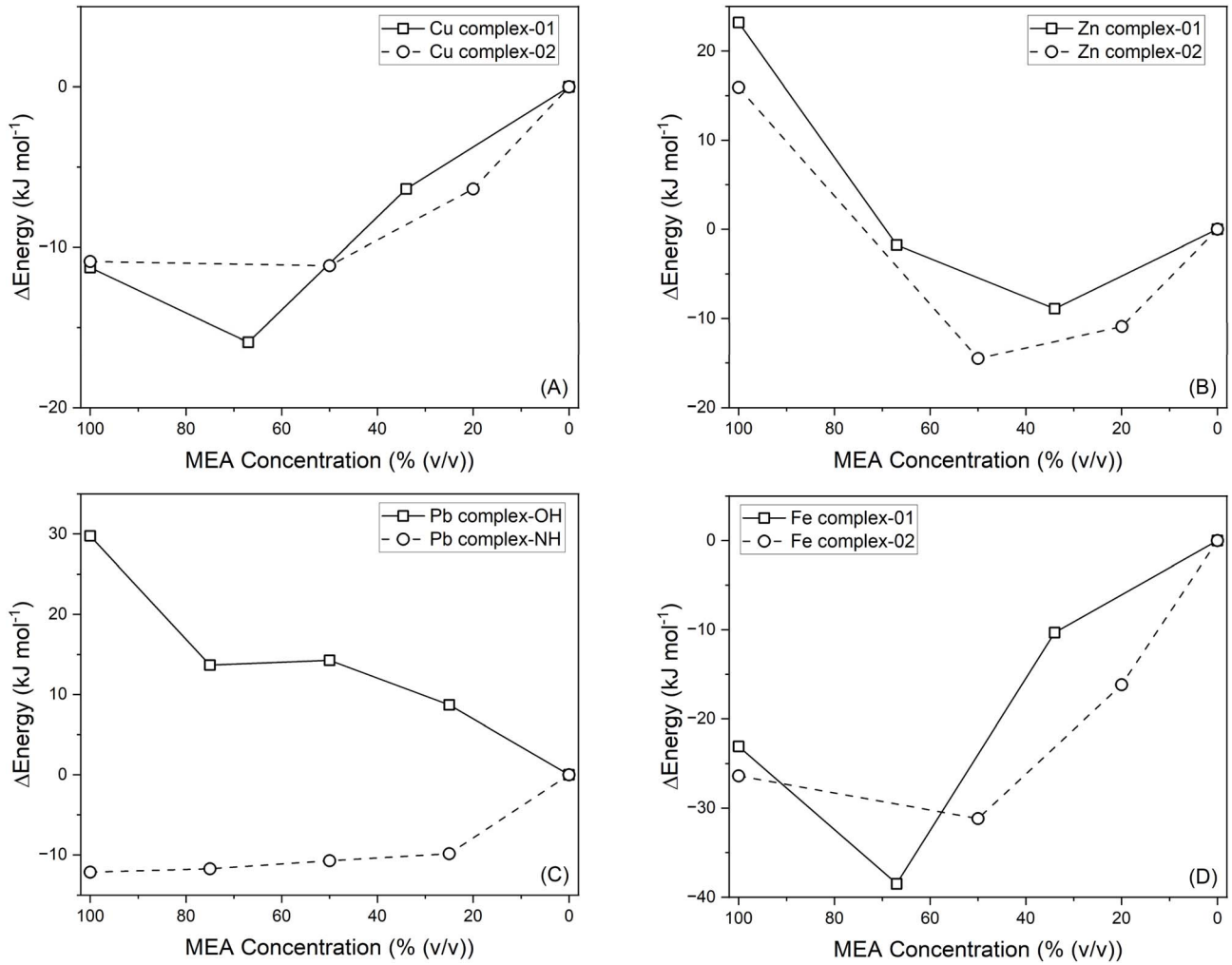

Fig. 8 ΔE_{BB} values for metal–MEA + water (A) copper, (B) zinc, (C) lead and (D) iron(II) cation complexes as a function of the MEA concentration in water. For Cu, Zn and Fe complexes with MEA and MEA + water, with respect to the structures reported in Fig. 7, complex-01 indicates monodentate coordination of MEA molecules with the metal atom (coordinated *via* the amine nitrogen atom) and complex-02 indicates the bidentate coordination of MEA molecules with the metal atom (coordinated *via* both the amine nitrogen atom and the hydroxy oxygen atom). Lines are a guide to the eye.

hydrated zinc and iron MEA + water complexes could therefore be attributed to the elimination of steric hindrance in these complex structures and also partly to the solvent medium effect, as reported by Kalidas *et al.*[46] Overall, similar to the lead MEA + water complexes, zinc and iron MEA + water complexes show a good semi-quantitative agreement between the experimentally determined ΔG_t and the calculated ΔE_{BB}, indicating that the complex binding energy has a strong contribution to the overall dissolution Gibbs free energy of the metal cations in the studied solvents. It is to be noted, however, that subtle differences between experimental dissolution Gibbs free energy (Fig. 6) and theoretical relative binding energies (Fig. 8) might stem for the influence of (i) explicit solvation, (ii) conformational variations in metal–MEA + water complexes stemming from explicit solvating molecules and to some extend on (iii) the choice of DFT functional/basis set; exploration of which are beyond the scope of the current work.

On the other hand, the Cu–MEA complexes, as reported in Fig. 8(A), are the only ones whose calculated binding energies deviate from the experimental trend, despite the fact that their optimized structures exhibit the expected coordination environment. Although it is well established that quantitative calculations on Cu(II) complexes are challenging, a systematic comparison with experimental observations is further complicated by the electronic-structure complexities and methodological limitations associated with open-shell Cu^{2+} coordination complexes. These include (i) the potential for spin-contamination, (ii) distortions in the optimized geometries arising from broken-symmetry solutions, and (iii) the difficulty of consistently identifying and comparing multiple low-energy conformers;[51,52] the optimized Cu–MEA structures, as reported in Fig. 7, do display the characteristic Jahn–Teller elongation (with axial Cu–O bond length of ≈2.2–2.3 Å; and equatorial Cu–O bond length of ≈2.0 Å). However, accurately capturing the relative energetics of d^9 Cu^{2+} complexes is intrinsically

challenging from single-reference DFT calculations. The negligible spin contamination observed in our calculations ($\langle S^2 \rangle = 0.7524$) indicates that the discrepancy with experimental observations (as reported in Fig. 6) does not originate from spin-state instability but rather from electronic-structure limitations associated with Cu^{2+}, including strong Jahn–Teller distortion, significant multireference character, and pronounced sensitivity to solvation and ligand-field effects. These factors often necessitate more advanced computational approaches – such as including higher-exchange or range-separated functionals (*e.g.*, PBE0, TPSSh, ωB97X-D), larger all-electron basis sets (*e.g.*, def2-TZVP or def2-TZVPP), explicit solvation tools, QM/MM embedding, or multireference methods such as CASSCF/NEVPT2 or DLPNO-CCSD(T) – combining some of which is necessary to obtain quantitatively reliable binding energies. While such methods could mitigate the discrepancy for Cu^{2+}, they introduce substantial computational complexity, particularly when examining multiple MEA concentrations, and therefore lie beyond the scope of the present study, which focuses on capturing qualitative trends rather than reproducing absolute thermodynamic values. Consequently, the correlations presented here are intended to be qualitative rather than quantitative as also the statistical indicators such as R^2 confirm that absolute numerical agreement with experiment is limited, even though the directional trends for Fe^{2+}, Zn^{2+}, and Pb^{2+} are reproduced. Accordingly, the DFT results are used here more towards rationalizing relative stability trends as a function of MEA concentration rather than to predict absolute thermodynamic quantities.

Based on the findings from the solubility tests of synthetic metal salts in the mixed system, leaching experiments of the roasted tailings were conducted using the combination of 90%, 70% and 50% (v/v) MEA and water. Within this chosen range the solubilities of copper, zinc and iron sulfate salts were increasingly higher than in pure MEA, whereas the solubility of $PbSO_4$ was higher than in pure water (Fig. 6). While the extraction efficiencies of copper and zinc from MW-assisted roasted tailings were not significantly affected by water addition to MEA in

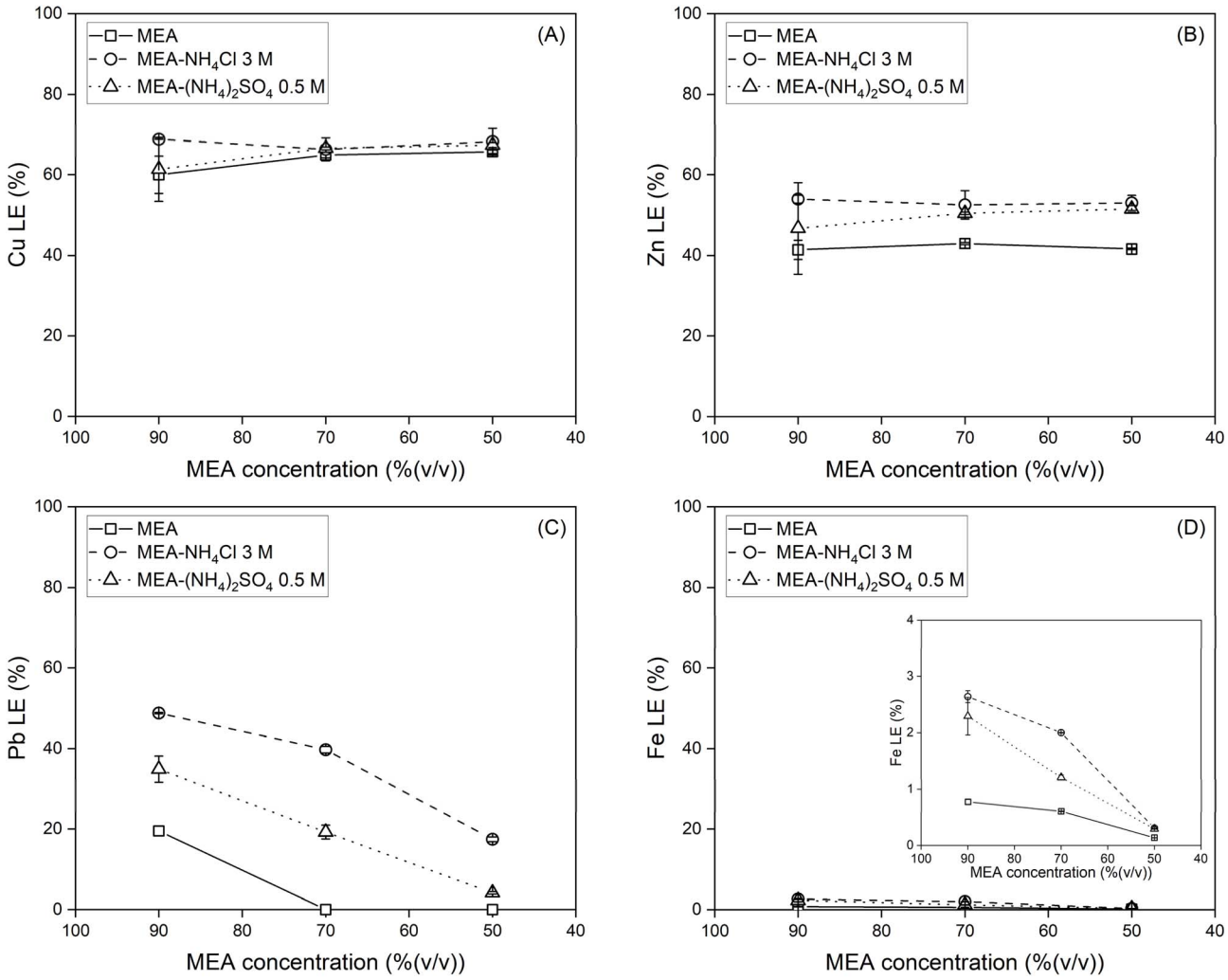

Fig. 9 Extraction efficiencies of targeted metals (A) copper, (B) zinc, (C) lead and metal impurities (D) iron from MW-assisted roasted sulfidic tailing (550 °C, 30 min) in MEA–water mixtures % (v/v) lixiviant ($T = 60$ °C; $t = 1$ h; L/S = 10 mL g^{-1}; stirring speed = 500 rpm) in the absence and presence of 3 M NH_4Cl or 0.5 M $(NH_4)_2SO_4$. Lines are a guide to the eye.

the studied v/v ratios (Fig. 9), those of lead and iron decreased upon increasing water addition. The addition of ammonium salts to the reaction mixture increased the extraction efficiencies of zinc and lead (Fig. 9). Contrary to pure MEA leaching, in the mixed MEA + water system, the addition of 3 M NH_4Cl increased the metal leaching efficiency more than 0.5 M $(NH_4)_2SO_4$. This effect was most strongly pronounced in the case of lead solubility, whereby it can be assumed that the presence of additional ammonia species allowed for an increased number of soluble lead complexes with ammonium groups that have a lower binding energy as discussed above and shown in Fig. 9(A).

Nevertheless, no increased dissolution of copper, zinc or lead was achieved through water addition to the leaching system. However, the insight gained from this study could be valuable when applied for the extraction of specific or certain valuable metals independently, rather than attempting to extract different valuable metals altogether from the complex matrix. For instance, the use of the mixed system MEA + water could be employed to extract copper and lead, while the use of pure MEA could be considered for lead extraction.

4. Conclusions

In this research, a combination of microwave heating pretreatment with solvometallurgical leaching is proposed using an MEA-based lixiviant for extracting copper, zinc, and lead from sulfidic tailings, with enhanced extraction efficiencies and/or selectivity. The optimal roasting conditions involved heating the tailings at 550 °C for 30 min in a microwave furnace, which resulted in the oxidation of the majority of the sulfide bearing minerals into their corresponding sulfate minerals. The leaching of the roasted tailings was then explored under various optimization parameters, including leaching in pure MEA, in MEA mixed with ammonium salts, and a mixed MEA–water system. The addition of ammonium chloride or ammonium sulfate to MEA enhanced the extraction efficiencies of the targeted metals. More specifically, leaching in MEA–$(NH_4)_2SO_4$ 0.5 M, achieved extraction efficiencies of 67% for Cu, 70% for Zn, 66% for Pb through mild temperature leaching at 60 °C for 1 hour. Of particular significance, is the substantial improvement in lead extraction (to ~66%) *via* this approach, when compared to water-leaching (of only ~1.5% from sulfidic tailings), as previously reported,[46] accentuating the potential of the MEA-based lixiviant as an alternative approach for the challenging task of lead extraction from lead(II) sulfate typically encountered in hydrometallurgical processing. Furthermore, MW-leaching also demonstrated the capability to enhance the dissolution of zinc through dissolution of remaining unroasted sphalerite phases from the tailings, thus improving the extraction efficiency of zinc compared to conventional leaching. However, copper extraction during MW-assisted leaching was lower compared to conventional leaching, possibly due to the adsorption of copper(II) ions onto magnesium ferrite phases formed during MW-leaching. Interestingly, adding water to the MEA system did not uniformly enhance the extraction of the targeted metals. While the addition of water to MEA did not strongly affect the copper and zinc extraction, it minimized the co-dissolution of iron impurities and had a negative impact on the extraction efficiencies of lead. Nonetheless, DFT calculated binding energies aligned qualitatively (directional trends) with the experimental Gibbs free energy of transfer for the dissolution of metal salts in MEA–water mixtures for Zn–, Fe– and Pb–MEA complexes, entailing that the complex binding energy has a strong contribution to the overall dissolution of Gibbs free energy of the metal cations in the studied solvents and thus providing insights on modulating the dissolution behavior of metal salts in MEA–water mixtures *via* modulating the binding affinities of metal–MEA–water complexes, which remains to be further explored.

Conflicts of interest

On behalf of all authors, the corresponding author states that there is no conflict of interest.

Data availability

The data supporting this article have been included as part of the supplementary information (SI). Supplementary information: Tables SI-1 and SI-2, Wiberg bond order variations for Zn–MEA complexes and Fe–MEA complexes, respectively. See DOI: https://doi.org/10.1039/d6ra00733c.

Acknowledgements

The authors thank Myrjam Mertens and Kosar Hassannezhad for their help with XRD and Rietveld analysis and Wendy Wouters and Warre Van Dun for experimental support. The research leading to these results has received funding from the European Community's Horizon 2020 Program under Grant Agreement no. 812580 (MSCA-ETN SULTAN). This publication reflects only the authors' view, exempting the Community from any liability.

References

1 L. Machiels, M. Frenzel, D. Goldmann, M. Illikainen and S. Pfister, *J. Sustain. Metall.*, 2021, **7**, 1440–1443, DOI: 10.1007/s40831-021-00468-7.

2 E.-L. Iatan, in *Phytorestoration of Abandoned Mining and Oil Drilling Sites*, 2021, ch. 16, pp. 373–408, DOI: 10.1016/b978-0-12-821200-4.00007-8.

3 L.-q. Lei, C.-a. Song, X.-l. Xie, Y.-h. Li and F. Wang, *Trans. Nonferrous Met. Soc. China*, 2010, **20**, 1488–1493, DOI: 10.1016/s1003-6326(09)60326-5.

4 J. Spooren, K. Binnemans, J. Björkmalm, K. Breemersch, Y. Dams, K. Folens, M. González-Moya, L. Horckmans, K. Komnitsas, W. Kurylak, M. Lopez, J. Mäkinen, S. Onisei, K. Oorts, A. Peys, G. Pietek, Y. Pontikes, R. Snellings, M. Tripiana, J. Varia, K. Willquist, L. Yurramendi and P. Kinnunen, *Resour., Conserv. Recycl.*, 2020, **160**, 104919, DOI: 10.1016/j.resconrec.2020.104919.

5 S. K. Sarker, N. Haque, M. Bhuiyan, W. Bruckard and B. K. Pramanik, *J. Environ. Chem. Eng.*, 2022, **10**, 107622, DOI: 10.1016/j.jece.2022.107622.
6 K. Binnemans and P. T. Jones, *J. Sustain. Metall.*, 2017, **3**, 570–600, DOI: 10.1007/s40831-017-0128-2.
7 M. Everaert, F. Guerrero, N. Kamariah and J. Spooren, *J. Sustain. Metall.*, 2021, **7**, 1537–1551, DOI: 10.1007/s40831-021-00382-y.
8 P. Xanthopoulos and K. Binnemans, *J. Sustain. Metall.*, 2021, **7**, 1565–1574, DOI: 10.1007/s40831-021-00463-y.
9 P. Luis, *Desalination*, 2016, **380**, 93–99, DOI: 10.1016/j.desal.2015.08.004.
10 M. Humar and B. Lesar, *Int. Biodeterior. Biodegrad.*, 2008, **62**, 46–50, DOI: 10.1016/j.ibiod.2007.06.017.
11 Y. Zhang, Y. Xu, S. Qiu and L. Yang, *J. Surfactants Deterg.*, 2013, **16**, 841–848, DOI: 10.1007/s11743-013-1488-7.
12 C. W. Davies and B. N. Patel, *J. Chem. Soc. A*, 1968, 1824–1828, DOI: 10.1039/j19680001824.
13 S. C. Rustagi and G. N. Rao, *J. Inorg. Nucl. Chem.*, 1974, **36**, 1161–1163, DOI: 10.1016/0022-1902(74)80233-2.
14 R. Tauler, E. Casassas and B. M. Rode, *Inorg. Chim. Acta*, 1986, **114**, 203–209, DOI: 10.1016/s0020-1693(00)86455-5.
15 D. M. Puente-Siller, J. C. Fuentes-Aceituno and F. Nava-Alonso, *Hydrometallurgy*, 2017, **169**, 16–25, DOI: 10.1016/j.hydromet.2016.12.003.
16 C. E. Cos-Castillo and J. C. Fuentes-Aceituno, *Miner. Eng.*, 2022, **186**, 107753, DOI: 10.1016/j.mineng.2022.107753.
17 D. A. Begum, M. F. Islam and R. K. Biswas, *Hydrometallurgy*, 1989, **22**, 259–266, DOI: 10.1016/0304-386x(89)90056-x.
18 P. Djurdjevic, J. Bjerrum, L. Melander, U. Wahlgren and C. I. F. Watt, *Acta Chem. Scand.*, 1983, **37a**, 881–890, DOI: 10.3891/acta.chem.scand.37a-0881.
19 E. Casassas, L. L. Gustems and R. Tauler, *J. Chem. Soc., Dalton Trans.*, 1989, 569–573, DOI: 10.1039/dt9890000569.
20 P. Caumul, K. Boodhoo, S. B. Burkutally, S. Seeruttun, N. Nammoya, N. Ramsahye and N. Joondan, *Res. J. Pharm., Biol. Chem. Sci.*, 2014, **5**, 494–509.
21 S. Subrahmanya, *J. Indian Inst. Sci.*, 1956, **38**, 245–248.
22 Krishna and M. Singh, *Indian J. Chem., Sect. A*, 1982, **21**, 595–598.
23 M. S. Masoud and A. A. Abdallah, *J. Chem. Eng. Data*, 2002, **27**, 60–62, DOI: 10.1021/je00027a019.
24 N. Kamariah, P. Xanthopoulos, K. Binnemans and J. Spooren, *Ind. Eng. Chem. Res.*, 2023, **62**, 12880–12890, DOI: 10.1021/acs.iecr.3c01834.
25 N. Kamariah, P. Xanthopoulos, J. Song, N. Pires Martins, J. Jordens, K. Binnemans and J. Spooren, *Ind. Eng. Chem. Res.*, 2024, **63**, 6110–6120, DOI: 10.1021/acs.iecr.4c00291.
26 N. Pires Martins, S. Srivastava, F. V. Simão, H. Niu, P. Perumal, R. Snellings, M. Illikainen, H. Chambart and G. Habert, *Sustainability*, 2021, **13**, 12150, DOI: 10.3390/su132112150.
27 N. Kamariah, D. Kalebic, P. Xanthopoulos, R. Blannin, F. P. Araujo, S.-F. Koelewijn, W. Dehaen, K. Binnemans and J. Spooren, *Miner. Eng.*, 2022, **183**, 107587, DOI: 10.1016/j.mineng.2022.107587.
28 M. Everaert, V. Lemmens, T. A. Atia and J. Spooren, *J. Cleaner Prod.*, 2020, **274**, 122628, DOI: 10.1016/j.jclepro.2020.122628.
29 D. Kalebic, W. Dehaen and J. Spooren, *Ind. Eng. Chem. Res.*, 2022, **61**, 13303–13313, DOI: 10.1021/acs.iecr.2c02043.
30 M. J. Frisch, G. W. Trucks, H. B. Schlegel, G. E. Scuseria, M. A. Robb, J. R. Cheeseman, G. Scalmani, V. Barone, G. A. Petersson, H. Nakatsuji, X. Li, M. Caricato, A. V. Marenich, J. Bloino, B. G. Janesko, R. Gomperts, B. Mennucci, H. P. Hratchian, J. V. Ortiz, A. F. Izmaylov, J. L. Sonnenberg, D. Williams-Young, F. Ding, F. Lipparini, F. Egidi, J. Goings, B. Peng, A. Petrone, T. Henderson, D. Ranasinghe, V. G. Zakrzewski, J. Gao, N. Rega, G. Zheng, W. Liang, M. Hada, M. Ehara, K. Toyota, R. Fukuda, J. Hasegawa, M. Ishida, T. Nakajima, Y. Honda, O. Kitao, H. Nakai, T. Vreven, K. Throssell, J. A. Montgomery Jr, J. E. Peralta, F. Ogliaro, M. J. Bearpark, J. J. Heyd, E. N. Brothers, K. N. Kudin, V. N. Staroverov, T. A. Keith, R. Kobayashi, J. Normand, K. Raghavachari, A. P. Rendell, J. C. Burant, S. S. Iyengar, J. Tomasi, M. Cossi, J. M. Millam, M. Klene, C. Adamo, R. Cammi, J. W. Ochterski, R. L. Martin, K. Morokuma, O. Farkas, J. B. Foresman and D. J. Fox, *Gaussian 16 Rev. C.01*, Wallingford, CT, 2016.
31 S. Grimme, *J. Comput. Chem.*, 2006, **27**, 1787–1799, DOI: 10.1002/jcc.20495.
32 E. D. Glendening, C. R. Landis and F. Weinhold, *J. Comput. Chem.*, 2013, **34**, 1429–1437, DOI: 10.1002/jcc.23266.
33 H. D. B. Jenkins and D. F. C. Morris, *Mol. Phys.*, 2006, **32**, 231–236, DOI: 10.1080/00268977600101741.
34 J. E. House, *Inorg. Nucl. Chem. Lett.*, 1980, **16**, 185–187, DOI: 10.1016/0020-1650(80)80118-8.
35 V. M. Petruševski, M. Monković and B. Šoptrajanov, *Chem. Educ.*, 2007, **12**, 71–74, DOI: 10.1333/s00897072012a.
36 S. Prasad and B. D. Pandey, *Miner. Eng.*, 1998, **11**, 763–781, DOI: 10.1016/s0892-6875(98)00061-2.
37 A. Ekmekyapar, N. Demirkıran, A. Künkül and E. Aktaş, *Braz. J. Chem. Eng.*, 2015, **32**, 155–165, DOI: 10.1590/0104-6632.20150321s00003211.
38 C. Wu, J. Tu, C. Tian, J. Geng, Z. Lin and Z. Dang, *Environ. Pollut.*, 2018, **235**, 11–19, DOI: 10.1016/j.envpol.2017.12.050.
39 S. Ilhan, S. G. Izotova and A. A. Komlev, *Ceram. Int.*, 2015, **41**, 577–585, DOI: 10.1016/j.ceramint.2014.08.106.
40 J. Xue, H. Zhang, J. Zhao, X. Ou and Y. Ling, *J. Magn. Magn. Mater.*, 2020, **514**, 167168, DOI: 10.1016/j.jmmm.2020.167168.
41 A. Ivanets, V. Prozorovich, T. Kouznetsova, T. Dontsova, O. Yanushevska, A. Hosseini-Bandegharaei, V. Srivastava and M. Sillanpaa, *J. Hazard. Mater.*, 2021, **411**, 124902, DOI: 10.1016/j.jhazmat.2020.124902.
42 A. I. Ivanets, V. Srivastava, M. Y. Roshchina, M. Sillanpää, V. G. Prozorovich and V. V. Pankov, *Ceram. Int.*, 2018, **44**, 9097–9104, DOI: 10.1016/j.ceramint.2018.02.117.
43 F. Liu, K. Zhou, Q. Chen, A. Wang and W. Chen, *J. Alloys Compd.*, 2019, **773**, 140–149, DOI: 10.1016/j.jallcom.2018.09.240.

44 Y. Feng, X. Lv, X. Ran, C. Jia, L. Qin, M. Chen, R. Qi, H. Peng and H. Lin, *J. Colloid Interface Sci.*, 2022, **608**, 749–757, DOI: 10.1016/j.jcis.2021.09.157.
45 Z. Li, B. Dewulf and K. Binnemans, *Ind. Eng. Chem. Res.*, 2021, **60**, 17285–17302, DOI: 10.1021/acs.iecr.1c02287.
46 C. Kalidas, G. Hefter and Y. Marcus, *Chem. Rev.*, 2000, **100**, 819–852, DOI: 10.1021/cr980144k.
47 P. Hess, *Nanoscale Horiz.*, 2021, **6**, 856–892, DOI: 10.1039/d1nh00113b.
48 L. M. Debefve and C. J. Pollock, *Phys. Chem. Chem. Phys.*, 2021, **23**, 24780–24788, DOI: 10.1039/d1cp01851e.
49 L. Gundelach, T. Fox, C. S. Tautermann and C. K. Skylaris, *Phys. Chem. Chem. Phys.*, 2021, **23**, 9381–9393, DOI: 10.1039/d1cp00206f.
50 S. J. Fox, J. Dziedzic, T. Fox, C. S. Tautermann and C. K. Skylaris, *Proteins*, 2014, **82**, 3335–3346, DOI: 10.1002/prot.24686.
51 F. Rodriguez, *Inorg. Chem.*, 2017, **56**, 2029–2036, DOI: 10.1021/acs.inorgchem.6b02677.
52 Z. Li, Z. Liu, S. Li, Y. Pei, D. Li, J. Mao, R. Zhou, C. Qiu, Y. Lu and B. Zhang, *J. Mater. Chem. A*, 2024, **12**, 15082–15089, DOI: 10.1039/d4ta01184h.